THE ANNALS OF "DUNAREA DE JOS" UNIVERSITY OF GALATI
FASCICLE XI – SHIPBUILDING. ISSN 1221-4620
2016

TRIAL COMPUTATIONS OF THE FREE-SURFACE FLOW AROUND A BULK CARRIER SHIP MODEL

Adrian Lungu
"Dunarea de Jos" University of Galati
Faculty of Naval Architecture
Domneasca Street, No. 47, RO-800008, Romania
E-mail:adrian.lungu@ugal.ro

ABSTRACT

A comprehensive viscous flow investigation around the Japan Bulk Carrier bare ship model is described in the present paper. The aim of the investigation is that of the necessity of calibration for the FINE^{TM}/Marine component of the NUMECA solver for further deeper numerical investigations. The global hydrodynamic resistance components, free-surface elevation, wake structure in the propeller plane as well as the trim and sinkage values are computed by using the ISIS-CFD numerical solver for the Reynolds-averaged Navier-Stokes equations in which the turbulence is modeled with the k-ω SST model. Comparisons with the experimental data are provided to validate the numerical approach.

Keywords: Numerical simulation**,** JBC, RANSE, free-surface flow, turbulence

1. INTRODUCTION

The end of the year of 2015 marked the seventh Workshop on CFD in Ship Hydrodynamics organized in Tokyo by the Japanese National Maritime Research Institute [1]. The purpose of the workshop was to assess the state of the art in CFD for hydrodynamic applications. As all the previous editions the claimed objective was to compare results of state-of-the-art numerical methods for a number of well specified test cases to assess the capabilities of the methods and to find the best way forward.

Three ship models were proposed to be studied by the community in sixteen different computational instances. Active researchers in the field worldwide were invited to provide computed results for a number of well specified test cases, the results were collected and reported so that comparisons between different methods could be easily made [2], [3]. The first hull considered was the JBC, i.e. Japan Bulk Carrier, which is a capesize bulk carrier equipped with a stern duct as an energy saving device, propeller and rudder. The National Maritime Research Institute, Yokohama National University and the Shipbuilding Research Centre of Japan were jointly involved in the design of the hull, the energy saving device and the rudder. Towing tank experiments were carried out at NMRI, SRC and Osaka University, which included resistance tests, self-propulsion tests and PIV measurements of stern flow fields. The hull design and measurements were conducted with the support of Class Nippon Kaiji Kyokai as part of a R&D program as acknowledged in [4] and [5].

The second hull considered was the already classic KCS, i.e. Kriso Container Ship, which was conceived to provide data for both explanation of flow physics and CFD validation for a modern container ship with a bulbous bow. The third hull was the Office of Naval Research tumblehome model 5613,

which is a preliminary design of a modern surface combatant, accessible for the community for fundamental research purposes.

The main reason for choosing in the study the JBC model was the great deal of experimental data, a fact that allows the author to perform all the numerical tests for a consistent verification and validation of the proposed theoretical approach. Aside of that, computing the flow around such a hull may be somehow difficult for gridding reasons since the bloc coefficient is so large, as one may see either in Fig.1 that emphasizes prominent geometric gradients around the fore and aft hydrodynamic shoulders, or in Table 1 where the main particulars of the full scale hull recommended in [1] are tabulated.

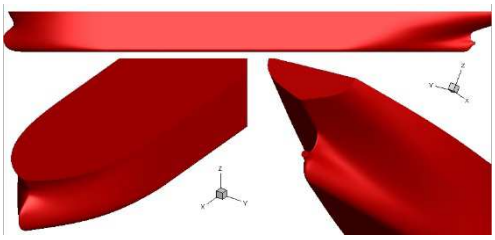

Fig. 1. JBC hull form

Table1. Full scale particulars of the JBC hull

Main particulars	unit	Value
Length between perpendiculars, L_{PP}	m	280.0
Breadth, B	m	45.0
Draft, T	m	16.5
Depth, D	m	25.0
Displacement, ∇	m^3	178369.9
Wetted area, S_0	m^2	19556.1
Block coefficient, C_B	-	0.8580

The geometry is susceptible to lead to important separations of the flow, therefore testing the accuracy of the available turbulence models becomes of a crucial importance for the simulation and that was another reason for the investigation [6]. Summing up, the objective of the present research is to investigate the capability of the code in relation to the computational fluid dynamics-based free-surface flow prediction. The ship running at the rather low Froude number of 0.142 is subjected to quasi-static sinkage and trim. The main focus of the present work will be on the free surface, the three dimensional vortical structure as well as on the validation of the two dimensional local flow quantities based on the available experimental data [4], [5] in an attempt to increase the reliability of numerical simulation tools in the ship design process by establishing robust modeling principles and uncertainty bounds. All the computations will be performed at a model scale of 1:40.

2. NUMERICAL APPROACH

The ISIS-CFD flow solver of the FINE^{TM}/Marine is employed in the study to investigate the flow field structure around the hull, based on a VOF approach. The numerical simulation of the free-surface is performed by using a free-surface capturing strategy [7]. The solver uses algorithms providing a strong pressure-velocity coupling for the RANSE, whereas an automatic grid adaptation by a posteriori error estimation is employed to resolve the local issues of the flow.

The simulation is accomplished in a global approach in which RANS equations written in respect to a Cartesian system of coordinates are solved. Since the aforementioned equations are well known by the reader they will be simply skipped here. No coordinate transformation is done in the solving process. The dependent variables of the set of equations are the velocity and pressure. The turbulence is treated by making use of the k-ω SST model. The forces integration is performed on the solid-surface cell based on the quaternions formulation. The full tensor is considered for the moments of inertia.

The integration in time is done in an Euler explicit way, whereas an upwind discretization scheme is used for the convective terms with a second order for the acceleration. Conservation applies to the mass and momentum and a Piccard model applies for

the linearization. The pressure-correction is imposed and the Krylov technique is used for the iteration of the solution. A non-structured grid is used for the discretization of the computational domain and hexahedral elements are used for that purpose.

A quasi-static approach is used to advance the solution in time. The initial conditions refer to the incoming flow velocity, pressure and turbulent viscosity only. The computational domain is limited at -0.75L_{pp} at the upstream where the velocity components, the pressure and the turbulent viscosity are imposed, whereas a Neumann condition is imposed for the pressure, as shown in Fig.2. At the downstream, which is located at 2.5L_{pp}, the velocity components and the turbulent viscosity are zero-extrapolated, whereas the pressure has the static value.

The no-slip condition is imposed on the hull. For the upper and bottom boundaries the pressure is prescribed at the static value. The symmetry condition is imposed on the centre plane of the ship, while on the far field, which is located at 2L_{pp} all the hydrodynamic parameters are extrapolated with zero-gradients. The flow starts from rest and it is accelerated within 10 seconds up to the given velocity.

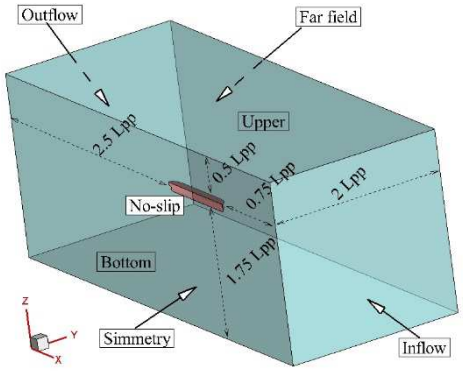

Fig. 2. Computational domain

2.1 GRID GENERATION

Whenever the turbulence quantities are computed, it is important to place the first grid within a certain y_{wall} to the solid wall where, for a viscous flow, the boundary layer displays high gradients. If an Euler computation is performed, no boundary layer exists and therefore the cell size near solid walls is of a less importance. On the opposite, in viscous flow case it is crucially important to have a sufficient number of grid points inside the boundary layer to capture properly those gradients. The local Reynolds number based on the wall variable y^+ is computed prior to the grid generation, to estimate an appropriate cell size y_{wall} for the Navier-Stokes simulations including turbulence. In the present study the gridding is done by using the Hexpress module of the FINE^{TM}/Marine, a generator which has not only direct CAD import capabilities, but it also allows the manipulation or the decomposition of the geometry. The automatic full hexahedral grids is possible as the buffer cell and boundary layer insertion for high quality cells in boundary layer regions. An automatic refinement procedure based on defined sensors either next to solid walls or inside specified area in the domain is also available [8]. Four grids varying from 3.16 to 19.3 million cells were generated for the sake of performing the grid convergence test for the solver. Fig.3 shows the 6.3 million cell computed grid for the extremities of the considered JBC hull.

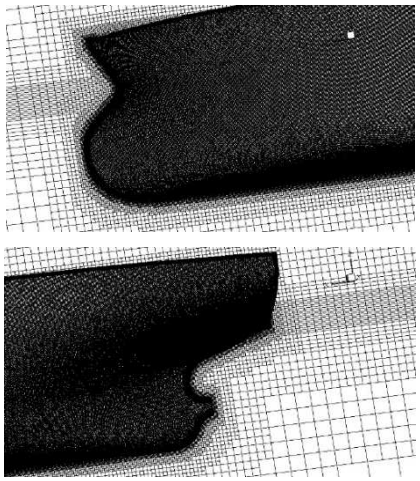

Fig. 3. Computational grid at the extremities of the hull

3. RESULTS AND DISCUSSIONS

The present paper will only discuss general issues of the JBC model resistance without focusing on the particularities of the flow around the hull, which will be treated separately later on. All the computations were carried out at a velocity of 1.179, which corresponds to a Froude number of 0.142 and to a Reynolds number of $7.46 \cdot 10^6$ on a computer with 12 cores with 96 GB of RAM.

An important issue of quasisteady or unsteady simulations is the correlation between the time step value and the grid size. It is well known that the parameter which links the two is the Courant number, whose value represents the minimal condition for the convergence of the numerical solution. It has been already proven that although it is a necessary condition, it may happen that having the Courant less than unity in time-marching computer simulations is not sufficient for the solution to reach the convergence. On the opposite, if the Courant number is greater than one the simulation will always produce misleading results.

In our particular case, a careful match between the time step value, which was chosen at a value ranging from $5e^{-5}$ to $1e^{-4}$ and the grid size could keep the Courant number less than unity during the whole simulation, as Fig.4 clearly proves.

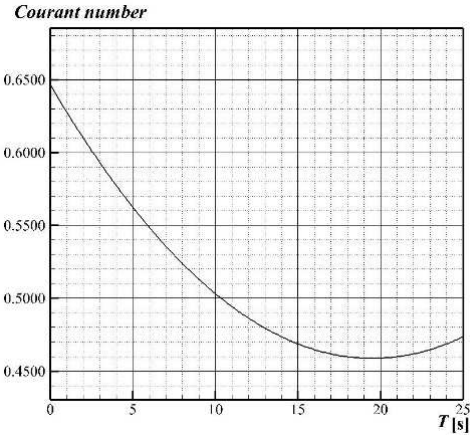

Fig. 4. Time variation of the Courant number

A series of comparisons between the numerical solution computational on the finest grid and the measured data in the towing tank at NMRI [4] will be proposed in the followings. The first comparison refers to the free-surface topology computed at T=25 and the corresponding experimental one. Although the theoretical solution seems to slightly underestimate the wave elevation, especially at the aft part of the body, the overall resemblance of the two is obvious, as it may be seen in Fig. 5. Comparisons between the values chosen for ten-point probes revealed differences ranging from 1.31 to 4.87 percent, values which may be considered as acceptable.

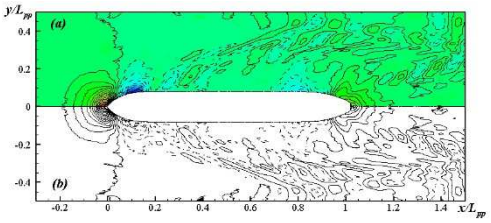

Fig. 5. Comparison between the free surface profile (a)-computed at T=25 sec and (b)-measured [4]

The next comparison between the numerical solution and the experiment refers to the wave cut along the hull computed at T=25 sec and the one measured by Hirata [4] is shown in Fig. 6. Although the resemblance may be considered as being satisfactory, rather significant differences are seen at about 0.825 of the L_{pp} as well as in the area of the first wave drought. These differences may suggest that the grid size was larger than the optimal one, despite of the refinement performed in those areas.

In the followings, two longitudinal wave cuts computed and measured at y/L_{pp}=0.1043 and 0.19 are respectively compared in figures 7 and 8. In both cases the agreement between the two data sets may be considered as acceptable for the area in which x/L_{pp} varies from 0 to 1 in terms of the magnitude and phase of the wave train. Seemingly, this is due to the suitable grid size which could be

imposed in the region corresponding to the hull.

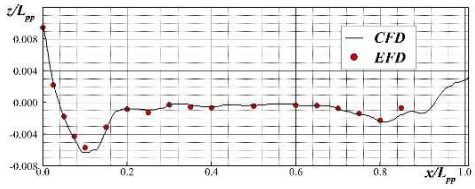

Fig. 6. Comparison between the wave cut along the hull computed at T=25 sec and measured [4]

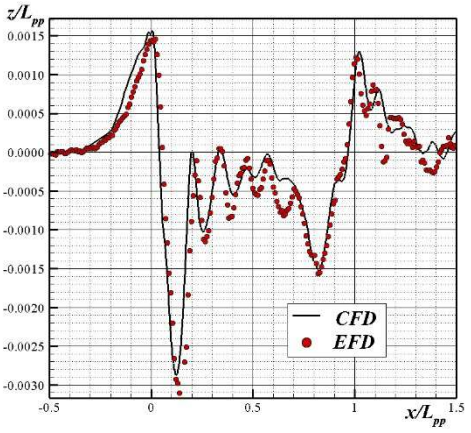

Fig. 7. Comparison between the longitudinal wave cut at y/L_{pp}=0.1043 computed at T=25 sec and measured [4]

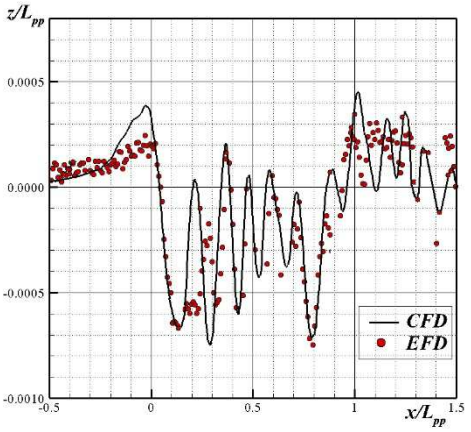

Fig. 8. Comparison between the longitudinal wave cut at y/L_{pp}=0.19 computed at T=25 sec and measured [4]

In terms of the ship resistance components, the time evolution of the solution computed on the 19.3 million cells grid is as shown in Fig. 9, which depicts the variation of its components as well. As it may be seen from the graph, a simulation time of 20 seconds may by good enough for the solution to be considered as being converged. Even though the computed results have proven that after 18.8 seconds the residuals of the main parameters of the flow kept remaining below of an order of 10^{-3}, which was imposed as a threshold for the solution of the numerical simulation [9] convergence, in the followings all the discussions will be done for the solution computed at T=25 sec. Fig. 9 shows that the viscous component of the total resistance computed for the half part of the hull (17.9826 N) is about four times larger than the pressure component due to the pressure (4.6155 N), a fact that is in a full concordance with the basics of the ship hydrodynamics. Since the wetted surface area estimated in respect to the length between perpendiculars for the static orientation in calm water is S/L_{PP}^2 = 0.2494, the corresponding non-dimensional resistance, the computed force coefficients variation in time is as shown in Fig. 10. The total resistance coefficient computed at T=25 sec is 4.242, a value which is about 1.414 % smaller than the EFD value of 4.289 [4].

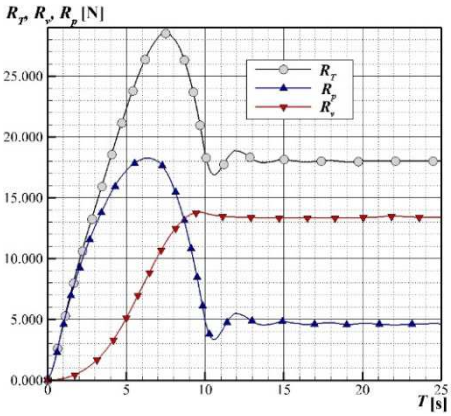

Fig. 9. Time variation of the resistance components computed for half of the body

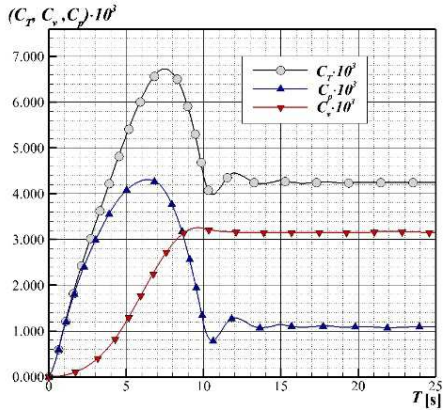

Fig. 10. Time variation of the resistance coefficients

As mentioned above, in the present study four simulations were performed on grids whose dimensions were 3.16M, 6.3M, 9.6M and 19.3M cells. The computed error for the total resistance coefficient in respect to the experiment ranged from 3.665% for the rougher to 1.414% that correspond to the finer one, values that may be considered as acceptable.

Another comparison is proposed in the followings for the sinkage expressed as a percentage of the length between perpendiculars. Fig.11 depicts the temporal variation of the relative sinkage computed on the 19.3M cells grid. Negative values denote a downward displacement.

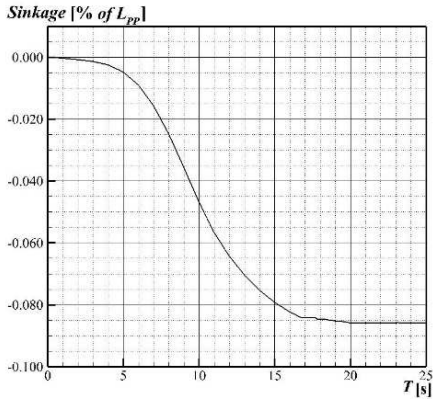

Fig. 11. Time variation of the relative sinkage

The computed value at convergence is –0.0856, while the corresponding measured one is –0.086, which denotes an error of 2.33%. Similarly, the trim computed on the same grid and expressed in respect to the length between perpendiculars is depicted in Fig. 12, which shows its variation in time. The negative values have the meaning of the bow down movement. The computed value is –0.1767, while the corresponding measured one is –0.18, which means that the computational error is 3.37%. The figure shows that the trim still varies after 25 seconds, a fact that may suggest that the computation should be continued for some more time.

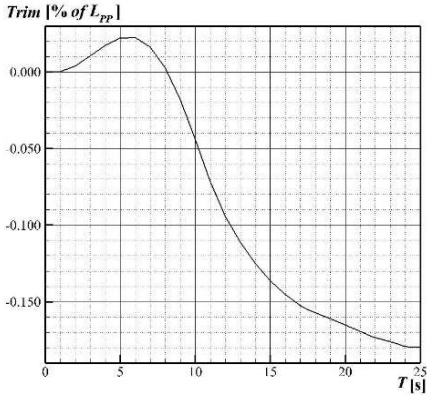

Fig. 12. Time variation of the relative trim

Usually the local flow analysis is uniquely based on the introspection in the flow characteristics at specific cross-sections where experiments are available. Although this procedure is still useful and necessary, it only provides a global insight into a certain number of measured parameters of the flow for each experimental cross-section [10], [11]. Under such circumstances an analysis based on the Q^* criterion is alternatively proposed in [3]. The criterion is defined as:

$$Q^* = Q\frac{L_{pp}^2}{U_{ref}^2}$$

where Q is the second invariant defined as follows:

$$Q = \frac{1}{2}\left(\Omega_{ij}\Omega_{ij} - S_{ij}S_{ij}\right)$$

Ω_{ij} in the equation above is the vorticity magnitude, while S_{ij} is the mean rate of strain tensor. The equation for Q is only valid for incompressible flows, i.e. for flows with divergence-free velocity field.

Following a procedure proposed by Visonneau et al. [12], figures 13 and 14 depict the isosurfaces of $Q^* = 25$ plotted at the extremities of the ship and colored by the non-dimensional helicity defined as follows:

$$He = \frac{\vec{U} \cdot \vec{\Omega}}{\left|\vec{U}\right| \cdot \left|\vec{\Omega}\right|}$$

Such an isosurface representation may provide a valuable information concerning the core of the vortices which are developed not only on the stern region, but also in the stream. Fig. 13 shows a bottom view of the bilge keel main vortices. Obviously, their intensity is rather significant, a fact which is expected to exert a negative influence on the propeller working conditions. The other vortical structures that developed in the proximity of the free surface are produced by the violent flow separation in the transom region. Although their intensity is lower, they contribute to the turbulent character of the flow with negative consequences on the wave component of the ship resistance.

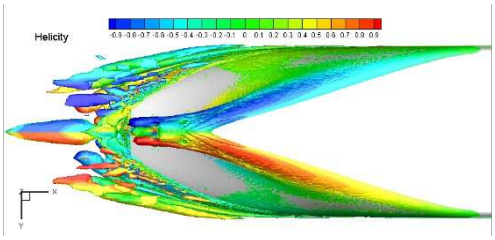

Fig. 13. Bottom view of the bilge keel vortices computed at T=25 sec

Similarly, the free-surface around the bow displays a region inside which the necklace vortex occurs at the intersection between the hull and the water surface. The oncoming boundary layer attached to the solid boundary encounters a strong adverse pressure gradient and separates ahead the bow. The two legs of the separated vortex roll around the bow being then washed in the downstream. If the velocity is larger than the critical value, the primary vortex generates a secondary one which is less intensive and possibly even a third one, as depicted in Fig. 14. The flow becomes fully turbulent and the bow wave eventually breaks. Obviously, this phenomenon also leads to an increase of the wave component of the hydrodynamic resistance therefore it should be avoided whenever possible by a careful choice of the hull forms there.

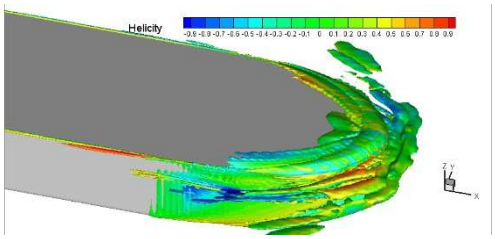

Fig. 14. Perspective view of the fore vortices computed at T=25 sec on the free-surface around the bow

4. CONCLUDING REMARKS

The 3D quasistatic free-surface flow around the JBC ship hull is numerically simulated to investigate the accuracy of the solver by making use of the experimental data existing in the public domain. The simulation is accomplished in a global approach in which the solution for the RANS equations written in respect to a Cartesian system of coordinates is advanced in time in a classical Euler manner.

Although not described in the present paper, a detailed grid convergence test was performed on the four grids in which the solution was computed. Since a detailed analysis of the local flow features was above the scope of the present paper, several quantitative comparisons with the experiments were performed for which the limits for the errors were less than 3.665%. This may emphasize not only the correctness of the numerical model, but also the overall accuracy of the solver.

The comparisons between the numerical solution of the simulation and the experimental data proved that the ISIS-CFD flow solver may reproduce with an encouraging accuracy the hydrodynamic behavior of a blunt ship hull if the computational input data are chosen correctly.

REFERENCES

[1]. **NMRI** (2015), *"Tokyo 2015 A Workshop on CFD in Ship Hydrodynamics"*, retrieved from http://www.t2015.nmri.go.jp/

[2]. **Larsson, L.,** http://www.t2015.nmri.go.jp/Presentations/Day1-AM4-JBC-Resist_etc-Larsson.pdf

[3]. **Visonneau, M.,** http://www.t2015.nmri.go.jp/Presentations/Day1-PM1-JBC-LocalFlow-Visonneau.pdf

[4]. **Hirata, N.,** http://www.t2015.nmri.go.jp/Presentations/Day1-AM2-JBC-TestData1-Hirata.pdf

[5]. **Hino, T.,** http://www.t2015.nmri.go.jp/Presentations/Day2-AM1-JBC-SpinclESD-Hino.pdf

[6]. **Duvigneau, R., Visonneau M. Deng, G.B.,** *"On the Role Played by Turbulence Closures in Hull Ship Optimization at Model and Full Scale"*, Journal of Marine Science and Technology, 8, 11–25, 2003.

[7]. **Queutey, P., Visonneau, M**., *"An Interface Capturing Method for Free-Surface Hydrodynamic flows"*, Computers and Fluids, 36, 1481–1510, 2007.

[8]. **Wackers, J., Deng, G.B., Guilmineau, E., Leroyer, A., Queutey, P., Visonneau, M.,** (2014), *"Combined Refinement Criteria for Anisotropic Grid Refinement in Free-Surface Flow Simulation"*, Computers and Fluids, 92, 209–222, 2014.

[9]. **Guha, A., Falzarano, J.,** *"Estimation of Hydrodynamic Forces and Motion of Ships with Steady Forward Speed"*, International Shipbuilding Progress, vol. 62, no. 3-4, pp. 113-138, 2015.

[10]. **Deng, G.B., Leroyer, A., Guilmineau, E., Queutey, P., Visonneau, M., Wackers, J., del Toro Llorens, A.,** *"Verification and Validation of Resistance and Propulsion Computation"*, Proceedings of Tokyo 2015 Workshop on CFD in Ship Hydrodynamics, 2015.

[11]. **Abbas, N., Kornev, N.,** *"Computations of the Japan Bulk Carrier using URANS and URANS/LES Methods Implemented into OpenFoam Toolkit"*, Proceedings of Tokyo 2015 Workshop on CFD in Ship Hydrodynamics, 2015.

[12]. **Visonneau, M., Deng, G.B., Guilmineau, E., Queutey, P., Wackers, J.,** *"Local and Global Assessment of the Flow around the Japanese Bulk Carrier with and without Energy Saving Devices at Model and Full Scale"*, Proceedings of the 31st Symposium on Naval Hydrodynamics, Monterey, California, 2016.

Paper received on September 15th, 2016

